IOSR Journal of Mechanical and Civil Engineering (IOSR-JMCE)
e-ISSN: 2278-1684,p-ISSN: 2320-334X, Volume 14, Issue 6 Ver. IV (Nov. - Dec. 2017), PP 18-29
www.iosrjournals.org

Effect of an Add-On Device on the Aerodynamic Characteristics of a 3-Dimensional Ahmed Body

A.O. Muritala[1†], H.A. Fatokun[1] and S.O. Obayopo[1]
[1] *Department of Mechanical Engineering, Obafemi Awolowo University, Ile-Ife, Osun State, 220005,Nigeria*

Abstract: *This study investigated the effect of add-on-device (side-view mirrors) on the aerodynamic characteristics of a 3-Dimensional Ahmed body using both numerical and experimental methods. It aims at controlling aerodynamic drag on vehicles by determining the optimum mirror position for a simplified vehicle geometry known as Ahmed body model. The rear slant angle of 25° has been used as a benchmark. The geometry is generated in ANSYS '14 design modeler with a single domain of air created surrounding the model after subtracting it from the air enclosure. The turbulent flows around the 3D Ahmed body model was solved using the realizable k-epsilon model with non-equilibrium wall function for near wall treatment with an inlet velocity of 40 m/s. For geometrical optimization, the following were used: distance between the attachment plate and the mirror ranges from 5-20 mm in an increment of 5 mm; height of the mirror foot ranges from 3-9 mm in an increment of 2 mm and the angle of inclination of the foot between -10° to +10° in an increment of 5°. The small scale prototype of Ahmed body was produced from a Prusa-i3 12 volts 3D printer. This was tested in a wind tunnel to determine the aerodynamic forces (drag and lift). The validation was done by comparing the small scale numerical modeling results with the experimental results obtained from the wind tunnel. The results from this study show that the position of the side-view mirror contributes to drag on the entire vehicle. Minimum drag coefficient C_D = 0.3022 and the corresponding lift coefficient C_L = 0.3410 was obtained at mirror position 20 mm foot length, 5 mm foot height and 10° angle of inclination. This position added 6% to the drag coefficient of the Ahmed body 25° model. The study concluded that the position of the side mirror contributes a significant effect when it comes to drag on the entire vehicle.*

Keywords*: Ahmed body, Drag coefficient, Lift coefficient, Turbulent flow, Aerodynamic forces and side mirror.*

Date of Submission: 12 -12-2017 Date of acceptance: 05-01-218

I. Introduction

Cars were mainly designed for high speed maneuver, comfort and safety before the oil crisis (Chien-Hsiung *et al*., 2009). However, automobile fuel efficiency standards have become more stringent due to the demand from governments and consumers leading to vast amounts of aerodynamic studies on vehicles (Jonathan *et al.,* 2015).Automotive aerodynamics comprises of the study of aerodynamics of road vehicles aiming at reducing drag, minimizing noise emission, improving fuel economy, preventing undesired lift forces and minimizing other causes of aerodynamic instability at high speeds.

A very important aerodynamic force is the drag which is caused by the pressure difference between the frontal and the rear end of the vehicle. It can be reduced by modification of the vehicle profile or systematic modification of the air flow system around the vehicle. It is necessary, at times, to generate down force to improve traction and thus cornering abilities. Another aerodynamic force is the lift which can be dangerous for an automobile, especially at high speeds. So, to maintain control by steering and braking, cars are designed so that the automobile exerts a downward force as their speed increases. However, increasing this downward force increases drag, which in turn, limits the top speed and increases fuel consumption. Hence, these two forces must be carefully balanced (Banga *et al*., 2015).

The air flow around a ground vehicle can be classified into two categories, internal and external flows. The external flow includes the underbody flows, flow over body surface and wake behind body. A wake is the region of re-circulating flow immediately behind a moving or stationary solid body caused by the surrounding fluid around the body. The external flow is responsible for over 85% of the drag force on the bluff body, and research shows that about 50% of the mechanical energy of the vehicle is wasted on drag at highway speed of nearly 88.5 to 96.5 kph (Agarwal, 2013).

Streamlined body design in a passenger car helps reducing the aerodynamics drag and eventually improves the engine mileage (Versteg and Malalasekera, 2007). However, in contrary, add-on devices or accessories attached to the body skin of a car cause unfavorable aerodynamics effects.

A real-life automobile is a very complex shape to model or to study experimentally. However, the simplified vehicle shape employed by Ahmed et al. (1984) generates fully three-dimensional regions of

separated flow which may enable a better understanding of such flows. Ahmed's body is 1044 mm long (*L*), 288 mm high and 389 mm width. The slant part is 222 mm long, whatever the angle. The bottom surface of the Ahmed body is located at 50 mm above the ground. This geometry is represented in Fig. 1. The flow around this body is strongly influenced by the angle of the rear slant surface, which indicates that the large portion of aerodynamic drag is generated by the development of three-dimensional vortex separation from the rear slant surface (Shamsuddin, 2009).

In this study, Ahmed Body has been selected due to its geometrical simplicity and availability of many experimental results. The flow velocity U_0 is 40 m/s and the kinematic viscosity of air is 15×10^{-6} m^2 s^{-1}. Then the Reynolds number, based on the body length, is 2.784×10^6. This simplified car model like Ahmed body or Society of Automotive Engineers (SAE) body makes it easy to relate the observed flow phenomena on a specific area and thus help to understand basic flow structures (Gopal *et al*., 2015).

The automobile side serves as an indirect vision that facilitates the observance of the traffic area adjacent to the vehicle which cannot be observed by direct vision. Being able to see what is behind the car is vital when reversing or changing lanes (Martin, 2011).

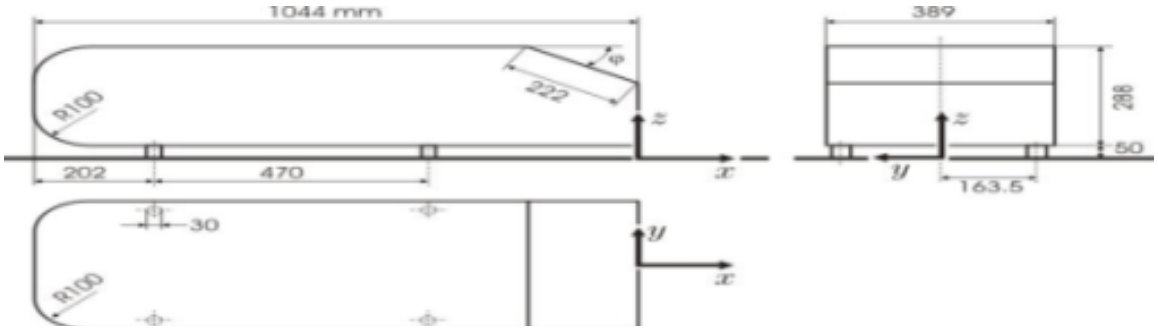

Fig. 1: Ahmed body geometrical descriptions (Ahmed et al., 1984)

There are many parts of the car that contribute to drag; one such part is the side view mirrors. The mirrors are often situated on, just in front of the driver's and front passengers doors. The mirror housing often holds the indicators, illumination features and a blind spot alarm. The flow around the mirror affects the aero acoustics of the mirror and is of great importance in minimizing mirror-glass vibration. The presence of the mirrors increases the total amount of drag by 2 to 7 percent (Huncho, 2005). This means that the mirrors contribute more to drag than they should in comparison to their size and the frontal area.

This paper investigates the effect of add-on device (side mirror) on the drag and lift coefficients of 3D Ahmed body. And it is expected to provide information for optimized geometry of add-on-device (side-view-mirrors) and positioning for optimal vehicle aerodynamics performance.

II. Methodology

2.1 Governing Equation

The flow around a car can either be laminar or turbulent depending on the speed of the vehicle. The present study investigates the effect of an add-on device on the aerodynamiccharacteristics of vehicles at high speeds. This is because aerodynamics effects are more critical at high Reynolds number (Chien-Hsiung et al., 2009). The governing equations are based on the basic equations obtained from mass and momentum balances. The mass conservation theory states that the mass will remain constant over time in a closed system. The mass conservation equation, also called the continuity equation can be written as:

$$\frac{\partial u}{\partial x}+\frac{\partial v}{\partial y}+\frac{\partial w}{\partial z}= \qquad 1$$

The terms on the left side of equation (1) are the velocity gradients in x, y and z directions which indicate the rate of change of flow velocity with position at a given time.

The conservation of momentum is originally expressed in Newton's second law which states that the forces acting on a particle are related to the resultant acceleration $\frac{\partial v}{\partial t}$ of the particle. The momentum equation can be written as:

$$\rho\left\{\frac{\partial u}{\partial t}+\frac{\partial(u^2)}{\partial x}+\frac{\partial(uv)}{\partial y}+\frac{\partial(uw)}{\partial z}\right\}= -\frac{\partial p}{\partial x}+\mu\Delta u \qquad 2$$

$$\rho\left\{\frac{\partial v}{\partial t}+\frac{\partial(vu)}{\partial x}+\frac{\partial(v^2)}{\partial y}+\frac{\partial(vw)}{\partial z}\right\}=$$

$$-\frac{\partial \mathrm{p}}{\partial \mathrm{y}}+\mu\Delta v \qquad 3$$

$$\rho\left\{\frac{\partial w}{\partial \mathrm{t}}+\frac{\partial(wu)}{\partial \mathrm{x}}+\frac{\partial(wv)}{\partial \mathrm{y}}+\frac{\partial(w^2)}{\partial \mathrm{z}}\right\}-\frac{\partial \mathrm{p}}{\partial \mathrm{z}}+\mu\Delta w \qquad 4$$

The terms on the left side of the equations (2, 3 and 4) are the acceleration terms. The right-hand sides are the pressure and the viscous forces respectively.

2.2 Computational Domain and Mesh Generation

The Ahmed body model with the slant angle of 25° was designed using AUTODESK INVENTOR'15. Dimensions remain identical with length, width and height of L = 1044 mm, W = 389 mm and H = 288 mm, respectively as shown in Figure 1. In ANSYS '14 Design Modeler, a single domain of air was created surrounding the body after subtracting it from the air enclosure. The enclosure has the dimensions of 5 m from front, 7.5 m from the rear and 3 m from the top. The model is 0.05 m above the bottom wall (Fig. 2). The mesh was generated using the ANSYS meshing. The meshing of the Ahmed body geometry and the solution domain with respects to the flow streams enables the proper discretization of the domain.. Fig. 2 shows the mesh generated for the single air body domain.

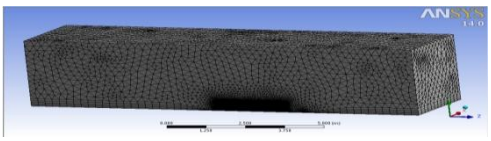

Fig. 2: Mesh Generated for Single Air Body Domain

To capture the flow physics around the car more accurately the mesh size kept near the car is fine and becomes coarse when go away from the car body and to capture the boundary layer around the Ahmed body model, multiple layers of fine element sizes are kept around the model by specifying the inflation layer method of first aspect ratio of 5, growth rate of 20% of 5 layers.

2.3 Computational Setup and Boundary Conditions

The present computational analysis requires the solver settings to be completed before starting the simulations. The solver settings include type of solver (3D or 2D), the viscous model, boundary condition and solution controls. The inlet of the virtual wind tunnel is indicated by the term 'Velocity inlet' while the outlet is termed 'Pressure outlet'. The boundary conditions are uniform velocity at inlet, uniform pressure at outlet.

2.4 Side Mirror Design

The first set of numerical simulation of flow around the Ahmed body 25° rear slant angle was done without side-view mirrors. This was done to obtain the value of the aerodynamics forces (drag and lift coefficients) on the 25° Ahmed body model without mirrors.

2.4.1 Measuring the side mirror area

To design the side-view mirror, three different car models namely Model A, Model B and Model C were selected as the base subject of the design. The dimensions of the three different Mercedes Benz Models; Model A, Model B and Model C including their side view mirrors were measured using calibrated measuring tape and Vernier caliper and their average values were calculated. The calculated values were then compared with the dimensions of the Ahmed body model to design the geometry of the side-view mirrors that will be equivalent to the size of the Ahmed body model. The details of the dimensions obtained from the measurement are presented in Table 2.

Table 2a: Dimensions of the car models used

Whole Car			
Car Model/Dimensions	Length (mm)	Height (mm)	Width
Model A	4080	1250	1500
Model B	4430	1200	1600
Model C	4460	1250	1500
Total	12970	3700	4600
Average	4323	1233	1533

Table 2b: Dimensions of the mirror

Side Mirror			
Car Model/Dimensions	Length (mm)	Height (mm)	Width
Model A	150	140	4
Model B	200	120	6
Model C	150	140	4
Total	500	400	14
Average	167	133	4.67

2.4.2 Determination of new mirror dimensions

The average dimensions of the car Model including their side-view mirrors were compared to that of the Ahmed body dimension to obtain the dimension of the new side view mirrors.

AB_L α AM_L

$AB_L = K \times (AM_L)$ 5

$A_L = K \times (NM_L)$6

AB_L - Average Mercedes-Benz length, AM_L - Average side mirror length, K = Constant of proportionality, A_L= Ahmed body length, NM_L= New mirror length.

From Table 2 consider a car model of total length 4323 and mirror length 167, the constant of proportionality in equation (5&6) is obtained as shown below:

4323 = K × 167

K = 25.86

For the Ahmed body

$A_L = K \times (NM_L)$ Therefore,

1044 = 25.86 × NM_L

NM_L = 40.37≈ 40mm

Similarly,

AB_H α AM_H

$AB_H = K \times (AM_H)$ 7A_H = K × (NM_H) 8

AB_H =Average Mercedes-Benz height, AM_H =Average side mirror height, K = Constant of proportionality, A_H = Ahmed body height, NM_H = New mirror height.

1233 = K × 133. K = 9.27

For the Ahmed body

A_H = 9.27 × NM_H

288 = 9.27 × NM_H.

NM_H = 31mm

2.4.3 Side Mirror Geometry Attachment and Position Optimization

The designed side mirror geometries were attached to the Ahmed body through an attachment plate and three different positions were simulated. Fig. 3 shows the 3D Ahmed body model with the attached side view mirrors. For the geometrical optimization, the gap distances (distance between the attachment plate and the mirror), height of the mirror foot and the angle of inclination of the mirror foot were varied. Four gap distances ranges from 5-20 mm in an increment of 5 mm were selected, four different height of the foot ranging from 3-9 mm in an increment of 2 mm and the angle of inclination of the foot between -10° to 10° in an increment of 5° were investigated.

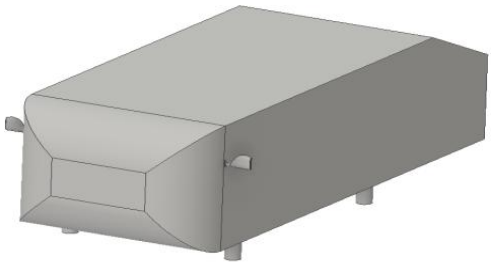

Fig. 3: 25° slant Ahmed model with side view mirrors

2.5. Experimental set-up

The validation of the numerical results is mostly done by comparison with results obtained through direct measurements from experiment. The most reliable information about physical phenomena is usually given by measurements but in certain situations, an experimental investigation which involve full scale model or equipment are either very expensive or difficult to perform or not possible at all. An alternative solution is to perform the experiment on a small scale model and extrapolate the results obtained to the full scale. The small scale Ahmed body model and the side mirrors at a ratio of 1 to 6 to the full scale model were produced separately using a Prusa-i3 12volts 3D printer. This model was produced based on the results of the numerical simulation obtained from computational analysis.The 3D printer puts ABS materials in ultra-thin layers onto a build tray until the part is completed.

2.5.1 Wind tunnel test

The KWASU Educational wind tunnel is of the open circuit type with a (30.4 cm x 30.4 cm x 60.96 cm) test section. Clean tunnel (empty test section) top speed is more than 145 mph (64.8 m/s) with near-infinite adjustability above 10 mph (4.47 m/s). The wind tunnel is shown in plate 1. Being an open circuit design, air is drawn from the surrounding environment (laboratory). This entering air first passes through a matrix of parallel passages called honeycomb. The honeycomb is about 10.16 cm long and serves to straighten the flow to eliminate flow angularity. The honeycomb does little to eliminate small eddies; the tunnel is equipped with two turbulence reducing screens immediately downstream of the honeycomb.

The Ahmed body prototype printed was mounted by fastening it to the sting Force/Moment balance as shown in plate 3. This prototype was equipped with a cylindrical socket; the socket was designed like the sting balance calibration bar. The forward portion of the socket was reamed to 23 mm in length, 9.5 mm in diameter for a snug fit and the rear portion was 45 mm in length and 15.9 mm in diameter to provide ample clearance. The 25° Ahmed body prototype was tested firstly without the side view mirror at zero degree angle of attack as shown in plate 2. The values of the normal and axial forces at 10 to 50 m/s in an increment of 10 m/s were obtained. The side view mirror prototypes were then attached to the 25° Ahmed body model by using glue gum and the values of the normal and axial forces were obtained at the same flow conditions.

Plate 1: Kwara State University (KWASU) Educational Wind Tunnel

Plate 2: Prototype of Ahmed body (25° slant angle) mounted in the wind-tunnel.

III. Results And Discussion

3.1. Validation of Numerical Results

The simulation results as well as the physics of this project was proved right by comparing the convergence of results, value of the drag and lift coefficients, velocity contour and the pressure distributions around the model 25° without add-on device (side view mirrors) with those of previous studies.

3.1.1 Convergence of result

Convergence means that the numerical solution should approach the exact solution of the differential equation at any point in the flow domain when Δx and Δt approach zero. In many numerical procedures, the concept of convergence is used differently. In iterative procedures, the residual is monitored which is the difference between the solution at one iterationand the next iteration for steady problems. Quoted from "Computational Fluid Dynamics (CFD) Blog- LEAP Australia & New Zealand Tips & Tricks Convergence and Mesh independent study", convergence can be generally defined by observing the behavior of the residual value. It is said that for steady state simulation we need to ensure that the solution satisfies the following conditions:

i Residual root mean square (RMS) error values have reduced to an acceptable value which is usually 10^{-4} or 10^{-5}.

ii Monitor points for our values of interest such as drag and lift have reached a steady solution i.e. the plot of the monitors begins and continue to oscillate about a repeated value.

The results of the Ahmed body models 25° without side mirrors have been proved valid when correlated with computational fluid dynamics (CFD) professional findings on convergence, drag coefficient and lift coefficient plots as shown in Fig. 4. In line with the above listed conditions, the drag and lift monitor commenced a steady solution at about 400-600 iterations which is maintained until the number of iteration was completed.

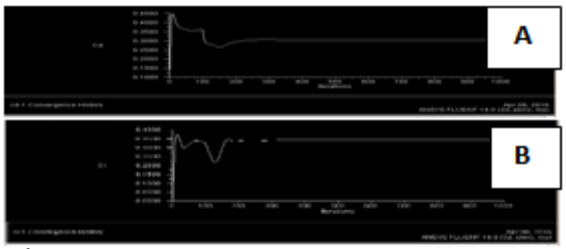

Fig. 4: Ahmed Body 25° Slant Convergence Plot. A - Drag coefficient and B - Lift Coefficient.

3.1.2 Drag and lift coefficients

The purpose of the numerical simulations without side-view mirrors for the Ahmed body 25° rear slant angle was to verify that the ANSYS Fluent physics used in this research is precise with respect to results of previous studies and to see the effect of side mirrors on the drag and lift coefficients. The result obtained is presented in Table 3. The drag coefficient (C_D) value for Ahmed body 25° obtained in this study was 0.2844 and the corresponding lift coefficient (C_L) was 0.3686. The drag coefficient value obtained was found to have some high level of proximity when compared with results reported by Ahmed *et al*., (1984), Braun *et al*., (2001) and Corallo *et al*., (2015).

Table 3: Drag Coefficient Values for Ahmed Body 25° Slant.

Research works	Drag C. (C_d)	Lift C. (C_L)
Present work	0.2844	0.3686
Ahmed et al., (1984)	0.2850	-
Braun et al., (2001)	0.2894	-
Corallo et al., (2015)	0.3210	-

3.1.3 Velocity contour and pressure distribution around the Ahmed body model

The velocity contour was observed to have the same pattern as that of the previous works. Figure 5(a) shows the velocity contour for the 25°rear slant anglecompared to Figure 5(b) which shows the velocity contours observed by Banga et al., (2015) at different rear slant angles of the Ahmed body model.

In Figure 5 the velocity distribution is non-uniform due to relative motion between different layers of the fluid. The green area corresponds to 40 m/s (free stream velocity) while blue area shows low velocity. At the interface between the fluid and the surface in relative motions, a velocity gradient exists in a direction perpendicular to the surface.This is because the particles of fluid adjacent to the surface are stationary, a condition known as "no slip" boundary condition.

The stagnation point at the front of the model indicates the region of zero velocity. At this point the convective terms of the momentum equations that govern the flow problem in all directions approaches zero and the pressure gradients equals the viscous forces on the surface.

Away from the surface, the fluid velocity rapidly increases which causes air flow to be divided between the upper and lower surface of the models. Again, as a result of stream- line curvature or change in geometry, the air accelerates and the air speed across the top is approximately 30% higher than the free stream air speed.

As the air continues to flow and makes its way to the rear, a notch is created by the rear slant owing to flow separation leaving a vacuum or void which the air is not able to fill properly. The dramatic change in

direction of flow due to the rear slant angle results in the formation of turbulent wake because the air is not able to make sharp turn and stick to the body as it supposed.

Figure 6a shows the pressure distribution around the model. There is extremely high pressure at the stagnation point due to zero velocity resulting from geometrical change. Gradual increase in velocity is noticed as the slant angle changes towards the rear. Banga et al., (2015) also observed similar pressure distribution around Ahmed body model at different rear slant angles (Figure 6b).

The pressure drag arises from the pressure difference or more generally from the non-uniform pressure distribution around the model. The stagnation pressure at the front of the body represented by the red area is more than that acting on the rear of the body, so resultant force acting on the body in the direction of relative motion exists. As the turbulent wake at the rear of the body becomes wider, there is a rapid increase in drag and decrease in the lift coefficient. The low pressure region at the rear of the body sucks the body backward and this result in more kinetic energy being dissipated and consequently more compensation power is required by the engine to propel the vehicle forward.

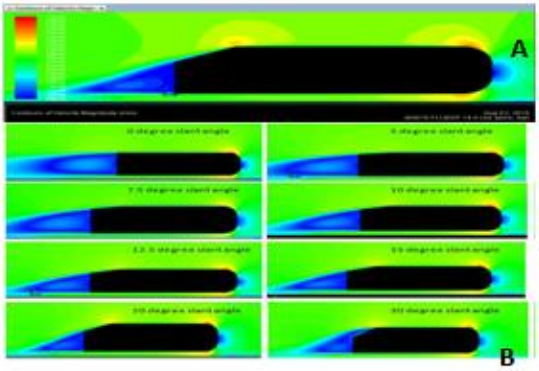

FIG.5: VELOCITY CONTOUR (A) 25° REAR SLANT ANGLE (B) AT DIFFERENT REAR SLANT ANGLES (BANGA ET AL., 2015).

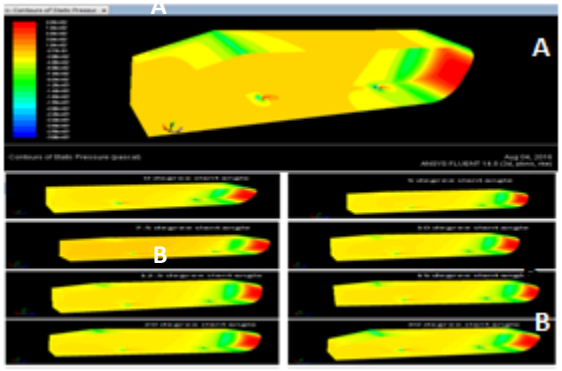

Fig. 6: Pressure distribution (a) 25° rear slant angle (b) At different rear slant angles (Banga et al., 2015)

3.2 Optimization of Side Mirrors Positions and Results.

The results of the 25° slant drag coefficient for different mirror positions are presented in Table 4. The variation in the values of drag and lift coefficients observed give a strong indication that there is mutual interaction between the varied parameters and each position contributes significantly to the drag and lift coefficients values. Fig.7 shows the plot of the drag coefficient at different mirror positions. This shows clear picture of the observed trends in relation to each parameter plotted. As the foot length increases from 5 mm to 20 mm, the values of the drag coefficient decrease and the trend was constant for all foot height and angles of inclination of the mirror foot.

However, a rapid increase in drag coefficient was observed at the mirror position 5 mm foot length, 5 mm foot height and 10° angle of inclination. This abnormal behavior was predicted to be because of closeness of the side mirror to the body of the model which does not allow free air flow between the body and the side mirror and therefore delayed the air speed around the mirror which leads to high pressure drag in the front of the model. The optimized position of the side mirror was observed at 20 mm foot length, 5 mm foot height and 10° angle of inclination. Drag coefficient C_D = 0.3022 and the corresponding lift coefficient C_L = 0.3413 was obtained at this position. The drag increase caused by an added add-on device (side-view mirror) at "A pillar" location would be around 1.7 times the drag the body would experience in an undisturbed flow field (Fox et al., 2004).

Table 4: Ahmed Body (slant angle 25°) Co-efficient of drag at 10° inclinations.

Length/Height	3mm	5mm	7mm	9mm
5mm	0.3101	0.3098	0.3101	0.3095
10mm	0.3051	0.3071	0.3070	0.3061
15mm	0.3057	0.3054	0.3056	0.3062
25mm	0.3026	0.3022	0.3033	0.3032

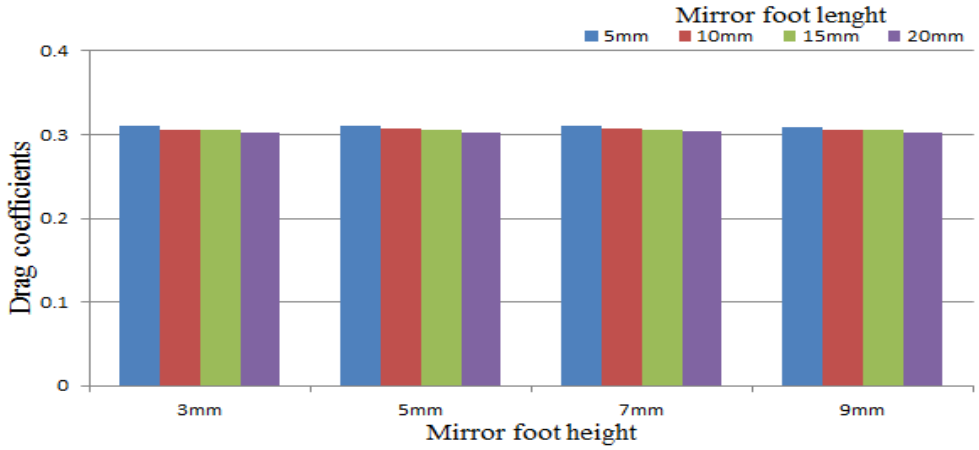

Fig.7: 25° Slant Drag Coefficients at 10° Angle of Inclination.

The drag increase caused by the optimized side mirror added to the Ahmed body 25° at "A pillar" location is around 1.07 times the drag experienced in an undisturbed flow field (i.e. the drag experienced without side-view mirror). This position only added 6 percent to the drag coefficient of the Ahmed body 25° slant which is in good agreement with Huncho, (2005), who stated that the mirror increase the total amount of drag by 2 to 7 percent.

The velocity contour observed at the position "A pillar" is shown in Fig.8 compared to the velocity contour of the Ahmed body 25° without mirror. The quantitative features of the flow observed are similar for both contours. The turbulence wake region seems to be larger due to the presence of side mirror which has delayed the acceleration of the flow at the upper and lower edges of the model. As the turbulence wake region becomes larger, boundary layer separation occur this resulted in increased drag and decreased lift coefficient. Fig. 9 shows the pressure distribution around the Ahmed body 25° with side mirror compared to pressure distribution around the Ahmed body without mirror.

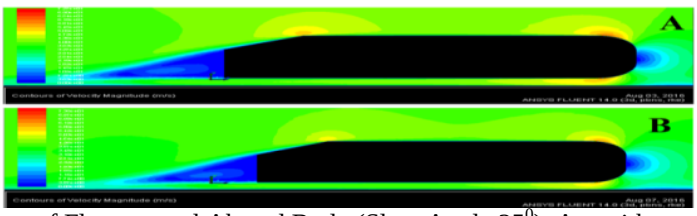

Fig. 8: Velocity Contour of Flow around Ahmed Body (Slant Angle 25^0), A – without mirror, B – with mirror

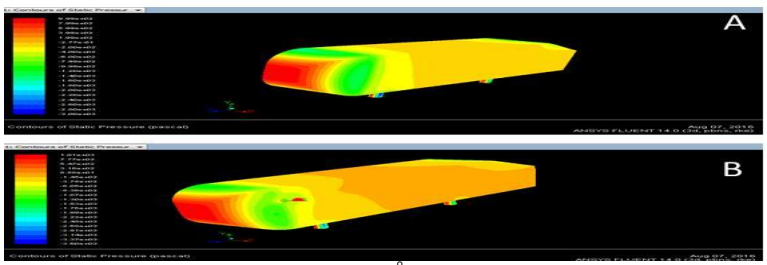

Fig. 9: Pressure Distribution around Ahmed Body 25° (A) Without side mirror and (B) with side mirror.

3.3 Experimental Results

The printed model tested in the wind tunnel give the values of the normal and axial forces at wind velocity of 10 to 50 m/s in an increment of 10 m/s at zero degree angle of attack. Table 5 shows the values of normal and axial forces obtained at 10 m/s to 50 m/s wind velocity for small scale 25° Ahmed body models. In

this Table, the normal and axial forces were found to be increasing with increase in wind velocity. This behavior is predicted to be because of increase in Reynolds number with increase in wind velocity. As the wind velocity increases, the flow region move from laminar to turbulence and as we continue at higher velocities wide turbulent wake is formed behind the body which increases the low pressure region formed behind the body. Similarly, Table 6 shows the values of normal and axial forces obtained after the side-view mirrors were attached. A further increase in these values with increase in wind velocity was observed.

3.3.1 Comparison of experimental and small scale simulation results

The values of normal and axial forces obtained from the experiment were converted to drag and lift forces using equations 9 and 10 and the corresponding drag and lift coefficients values were obtained using equations 11 and 12.

Drag force = $N\sin\alpha + A\cos\alpha$ 9

Lift force = $N\cos\alpha - A\sin\alpha$ 10

Where α = Angle of attack. N = Normal force. A = Axial force

$F_D = \frac{1}{2}\rho C_d U^2 A$ 11

$F_L = \frac{1}{2}\rho C_L U^2 A$ 12

Where ρ, U and A are the fluid density, flow velocity and area respectively.

Table 5: Experimental results of small scale 25° Ahmed.

Velocity (m/s)	Axial force	Normal force
10	0.155	0.180
20	0.478	0.602
30	0.984	1.272
40	1.622	2.167
50	2.297	3.244

Table 6: Experimental Results of Small Scale 25° Ahmed Body with Side Mirrors.

Velocity (m/s)	Axial force	Normal force
10	0.248	0.153
20	0.602	0.499
30	1.074	1.043
40	1.775	1.811
50	2.722	2.724

Numerical simulation results of the small scale models carried out at a velocity of 10 to 50 m/s were compared with the experimental values. Table 7 shows both the experimental and numerical results obtained without side mirrors while Table 8 shows the experimental and numerical results obtained with the side mirror attached. The decrease in drag and lift coefficient values with increase in flow velocity observed in this Table indicate an increase in drag and lift forces with increase in flow velocity. Fig.15 and 16 shows the plot comparing the drag and lift coefficients of both experimental and numerical results of small scale Ahmed body 25° without and with side mirrors. This Figure shows the relationship between the experimental and numerical results obtained at 10 to 50 m/s which give a clear picture of how the drag and lift coefficients values decreases with increase in flow velocity. The small deviation observed in the results is probably because of the ground effect in the numerical simulations which is not in the experimental setup because of the way the model was mounted in the wind tunnel.

Table 7a: Comparison of Numerical and Experimental Drag force of Small Scale 25° Ahmed Body without side mirrors

Velocity (m/s)	Experimental Drag force	Numerical Drag force
10	0.7912	0.7894
20	0.6100	0.7066
30	0.5581	0.6850
40	0.5175	0.6722
50	0.4853	0.6646

Table 7b: Comparison of Numerical and Experimental Lift force of Small Scale 25° Ahmed Body without side mirrors

Velocity (m/s)	Experimental Lift force	Numerical Lift force
10	0.9188	0.8528
20	0.7682	0.7646
30	0.7214	0.7718
40	0.6913	0.7518
50	0.6623	0.7480

Table 8a: Comparison of Numerical and Experimental drag force of Small Scale 25° Ahmed Body with Side Mirrors

Velocity (m/s)	Experimental Drag force	Numerical Drag force
10	1.1660	0.9172
20	0.7079	0.8370
30	0.5613	0.8152
40	0.5218	0.8036
50	0.5121	0.7964

Table 8b: Comparison of Numerical and Experimental lift force of Small Scale 25° Ahmed Body with Side Mirrors

Velocity (m/s)	Experimental lift force	Numerical lift force
10	0.7197	0.7122
20	0.5868	0.6384
30	0.5451	0.6288
40	0.5324	0.6224
50	0.5125	0.6166

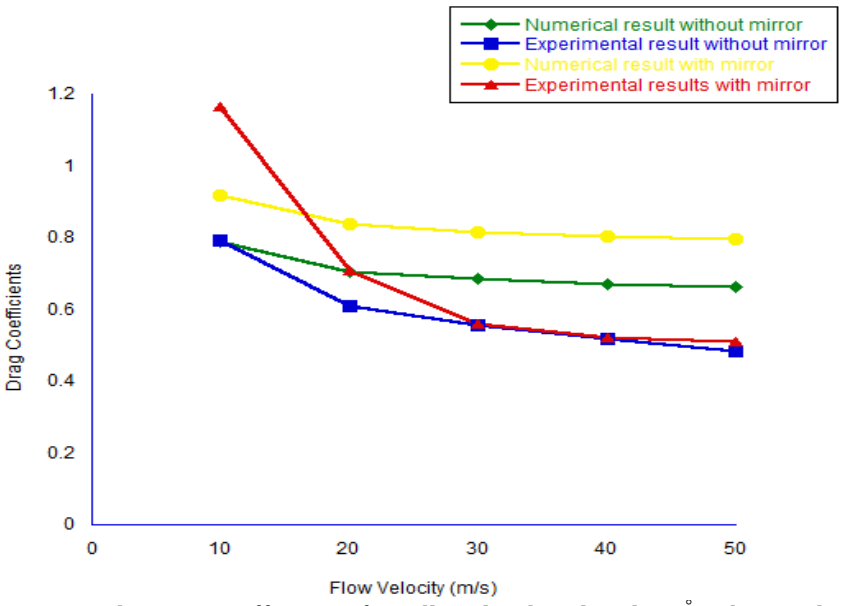

Fig. 10: Graph Comparing the Drag Coefficients of Small Scale Ahmed Body 25° without and with side mirror.

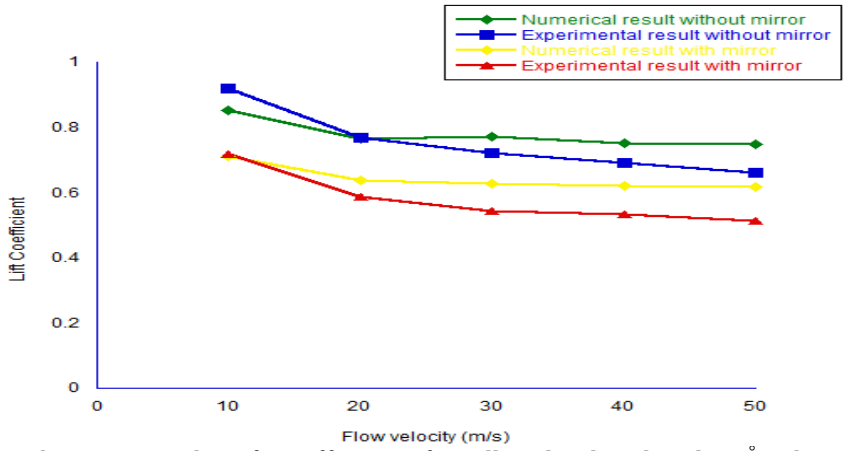

Figure 13: Graph Comparing the Lift Coefficients of Small Scale Ahmed Body 25° without and with Side Mirror.

III. Conclusions

This study presents an investigation of the effect of add-on device (side-view mirror) on the aerodynamic characteristics of a 3-dimensional Ahmed body.The research has found that the position of the side mirror contributes a significant effect when it comes to drag on the entire vehicle. The interaction that the longitudinal "A-pillar" vortices have with the flow over the rear slant is evident by the flow pathlines observed in Figs. 10 and 13, the increase in "A-pillar" vortices as a result of the changes in mirror foot length, mirror foot height and angle of inclination causes unstable flow reattachments and contributed to the position of flow separation. Hence, a total of 80 different mirror positions were simulated on the geometry to determine an optimized position of the side mirror.

Based on the simulation results generated, the following conclusions can be drawn for 25° Ahmed body;

a) The minimum drag coefficient C_d = 0.3022 and the corresponding lift coefficient C_L = 0.3413 was obtained at the mirror position 20 mm foot length, 5 mm foot height and 10° angle of inclination. This position only added 6% to the drag coefficient of the Ahmed body 25° model and therefore should be considered.

b) The mirror position 5mm foot length 5mm foot height and -10° angle of inclination may not be considered because of the higher drag coefficient added to the Ahmed body 25° model.

Reference

[1]. AEROLAB Educational Wind Tunnel (EWT) Operations Manual for Colorado Mesa
[2]. University & University of ColoradoBoulder(2012). http://www.aerolab.comAccessed: May 25th 2016.
[3]. Agarwal, R.K., (2013). Sustainable Ground Transportation, Challenges and Opportunities. Department of Mechanical Engineering & Materials Science, Washington University in St. Louis, MO 63130, USA
[4]. Ahmed S.R., Ramm G. and Faltin G. (1984). Some Salient Features of the Time-AverageGround Vehicle Wake, SAE-Paper, 840300.
[5]. Ahmed S.R., 1981. Wake Structure of Typical Automobile Shapes. Transactions of the ASME, Journal of Fluids Engineering, 103: 162 – 169.
[6]. Asykin, M.T., (2012). "CFD Simulation of Vortex Induced Vibration of a Cylindrical Structure"
[7]. Baker C.J., (2010). The Flow around High Speed Trains. Journal of wind Engineering and Industrial Aerodynamic,98:277-298.
[8]. Banga S., Zunaid Md., Ansari N.A, Sharma S., and Dungriyal R.S., (2015). CFD
[9]. Simulation of Flow around External
[10]. Vehicle: Ahmed Body. Journal of Mechanical and Civil Engineering (IOSR-JMCE), 12: 87-94.
[11]. Braun M., Lanfrit M., Cokljat D., (2001). Simulation of the Ahmed body 9th ERCOFTAC/ IAHR Workshop on Refined Turbulence Modelling. Chien-Hsiung Tsai, Lung-Ming Fu, Chang-Hsien Tai, Yen-Loung Huang and Jik-Chang Leong, (2009). Computational Aero-acoustic Analysis of a Passenger Car with a Rear Spoiler. Journal of Applied Mathematical Modeling 33:3661-3673. Elsevier.
[12]. Coasta Brainne, (2015). Studying the Flow around a Car using Ahmed Body.Comsolblog https://www.comsol.com/blogs/studying-the-airflow-over-a-car-using-an-ahmed-body/ Accessed: 13th Jan., 2016.
[13]. Corallo M., Sheridan J., Thompson M.C., (2015). Effect of Aspect Ratio on the Near-wake Flow Structure of an Ahmed Body. Journalof Wind Engineering and Industrial Aerodynamics 147: 95-103. Elsevier.
[14]. Douglas J.F., Janusz M., Gasiorek J.A., Swaffield L., Jack B., (2005). Fluid Mechanics. Fifth Edition. Pearson Prentice Hall England.
[15]. Fox R.W., McDonald A.T. and Pritchard P.J., (2004). Introduction to Fluid Mechanics. Sixth Edition John. Wiley and Sons. Inc.United State.
[16]. Gopal S., Aniruddha J., and Kishor N., (2015). Numerical Investigation of the Driver Car Model using Open Source CFD Solver OpenFOAM. Tata Consultancy Services, Pune. India.
[17]. Guilmineau E. (2008). Computational Study of flow around a Simplified Car Body. Journalof Wind Engineering and IndustrialAerodynamics 96: 1207 – 1217.

[18]. http://www.leapaust.com.au/Computatioal Fluid Dynamics (CFD) Blog- LEAP Australia &New Zealand Tips & Tricks Convergence and Mesh independent study.
[19]. Hucho W.H. (2005) Aerodynamics of Road Vehicles Wieweg + Teubbner, Fifth Editon 2005.
[20]. Jonathan M., Erik F., Gregory R., Rajan K., Kunihiko T., Farrukh A., Yoshihiro Y. and Kei, M. (2015). Drag Reduction on a Flat Back Ground Vehicle with Active Flow Control. Journal of Wind Engineering andIndustrial Aerodynamics 145 (2015) 292-303.Elsevier.
[21]. Marco Lanfrit, Version 1.2 (Feb., 9th 2005). Best Practice Guidelines for Handling Automotive External Aerodynamics with Fluent. Fluent Deutschland GmbH Birkenweg 14a 64295 Darmstadt/Germany.
[22]. Martin, O., (2011). Designing and Optimizing Side View Mirrors. Department of Applied Mechanics Division of Vehicle Engineering and Autonomous Systems Chalmers University of Technology Goteborg, Sweden.
[23]. .Post F.H., Walsum, T. (1993). Fluid Flow
[24]. Visualization van.Focus on Scientific Visualization Hagen, H. Müller, G.M.Nielson (eds.), Springer Verlag, Berlin, pp. 140 (ISBN 3- 540-54940-4)..
[25]. Pramod N.K., 2009. CFD Study of Drag Reduction of a Generic Sport Utility Vehicle.Department of Mechanical Engineering. California State University.
[26]. Shamsuddin, M.K., (2009). Aerodynamic Study of Vehicle Drag Based on Bluff Body. Faculty of Mechanical Engineering University of Malaysia, Pahang.
[27]. Versteeg H.K. and Malalasekera W., (2007). An Introduction to Computational Fluid Dynamics: The Finite Volume Method.Pearson Prentice Hall England.

A.O. Muritala "Effect of an Add-On Device on the Aerodynamic Characteristics of a 3-Dimensional Ahmed Body ." IOSR Journal of Mechanical and Civil Engineering (IOSR-JMCE) , vol. 14, no. 6, 2017, pp. 18-29